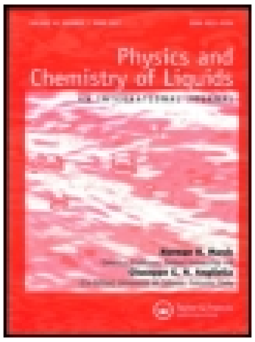

Physics and Chemistry of Liquids
An International Journal

ISSN: 0031-9104 (Print) 1029-0451 (Online) Journal homepage: http://www.tandfonline.com/loi/gpch20

The structuring in mixtures with acetone as the common solvent

Martina Požar & Larisa Zoranić

To cite this article: Martina Požar & Larisa Zoranić (2019): The structuring in mixtures with acetone as the common solvent, Physics and Chemistry of Liquids, DOI: 10.1080/00319104.2018.1564305

To link to this article: https://doi.org/10.1080/00319104.2018.1564305

PHYSICS AND CHEMISTRY OF LIQUIDS
https://doi.org/10.1080/00319104.2018.1564305

ARTICLE

The structuring in mixtures with acetone as the common solvent

Martina Požar[a,b] and Larisa Zoranić[a]

[a]Department of Physics, Faculty of Science, University of Split, Split, Croatia; [b]Faculté des Sciences, Laboratoire de Physique Théorique de la Matière Condensée (UMR CNRS 7600), Sorbonne Université, Paris Cedex 05, France

ABSTRACT
A molecular dynamics study of binary mixtures with acetone and different non-polar solutes (benzene, pentane and carbon tetrachloride) was undertaken. Through the analysis of different structural features, Kirkwood–Buff integrals, as well as energy distributions the weak nonideality is observed, governed mainly by the acetone's interactions. The excess thermodynamic properties highlighted that the subtle balance between unfavourable energetic and favourable entropic contributions promotes mixing. The solutes, despite showing differences, exhibit globally similar behaviour. The characteristics of these mixtures contrast those of the acetone-methanol mixtures, which exhibit more complex structuring, dictated primarily by the methanol molecules.

ARTICLE HISTORY
Received 17 September 2018
Accepted 26 December 2018

KEYWORDS
Binary mixtures; molecular dynamics; acetone; non-polar solute; weak nonideality

1. Introduction

Acetone is commonly used as a solvent for organic and inorganic matter [1,2]. The molecules of acetone consist of the bivalent carbonyl group attached to two methyl substituents [3] and possesses a significant dipolar moment [4] due to the electronegativity difference between the carbon and oxygen. The dipolar charge distribution as well as acetone's molecular topology favour the associations of the acetone molecules into short-lived dimers [5,6]. It is still discussed how the acetone interactions contribute to the overall mixing scheme when different types of solutes are added. Namely, it is reported by both experiments and simulations that the miscibility conditions in acetone mixtures are dependent on the very subtle balance between energetic and entropic contributions [7,8], hinting at the importance of the acetone associations. In the case of acetone mixing with polar or amphiphilic molecules, it is interesting to understand why the bonding of the C=O group is less effective in creating a favourable energy of mixing with the other hydrogen-bonding molecules. The reason behind might be the strongly associated structure beyond first neighbours observed in hydrogen-bonded systems. For example, in the study of the acetone–methanol clusters, Kollipost et al. suggested that the molecular pair interaction between acetone and methanol is very attractive, but it becomes less attractive as the cluster size increases [9]. Therefore, the immiscibility is created not by the unfavourable pair interactions, but rather by the non-favourable mixing of the larger molecular associations when compared to the self-association.

A simpler structural organisation is observed for the binary mixtures of acetone and non-polar solutes; however, its description is not without challenges. Investigations of acetone in carbon tetrachloride imply that, at low acetone concentrations, acetone molecules will tend to associate into dimers [10–12]. Other studies of acetone in non-polar solutes, such as cyclopentane and cyclohexane, suggest weaker dimer formation at higher acetone content [13,14]. A study of another dipolar molecule, dimethyl sulfoxide (DMSO), which shares the same interaction as acetone, but with

CONTACT Larisa Zoranić larisaz@pmfst.hr
Supplemental data for this article can be accessed here.

the different molecular topology [4], in benzene and carbon tetrachloride confirms that DMSO forms dimers when mixed with both solutes [15]. Also, experimental results of dynamical properties have shown that acetone–benzene and acetone–carbon tetrachloride have a marked minimum in the diffusivity–composition curves [16], which differ from the monotonous functions ideal systems have [17]. This behaviour in the acetone–benzene binary mixture is further extended when alcohols are added into the mixture [18]. The reported findings highlight the fact that acetone solutions, including those with the non-polar solutes, are not quite in the simple mixture category.

In this article, we will explore further the weak nonideality of the acetone solutions targeting several issues: to describe the molecular structuring on the level of particle and energy distributions; to define how mixing differently shaped non-polar solvents with acetone influences the structural organisation; to differentiate the type of disorder in acetone-polar and acetone non-polar solutions. The new perspectives gained while investigating complex mixtures will be of particular use while revisiting simpler systems with acetone as the common solvent.

The importance of molecular interactions in generating different types of disorder has been explored in some of our previous papers [19,20]. The complex disordered systems, as those including water or alcohols, showed pronounced signatures of micro-heterogeneity, i.e. the segregation of two species on the molecular level [21,22]. Although the acetone–benzene mixture exhibited features that could be placed in between simple and complex disorder, it still leaned more towards the category of simple disorder. Going one step further, we have also noticed that in mixtures of alcohols and non-polar solutes of different molecular shapes, the shape of the solute has no influence on the characteristics of the mixture [20]. The interactions of the associating species are paramount, leading the species to self-segregate and therefore produce a micro-heterogeneous mixture, regardless of the non-polar solute.

The behaviour of realistic acetone is reproduced fairly well with some of the well-known force fields such as OPLS and TraPPe [23,24], which use the partial charges model for representing the acetone electrostatic interaction. Recently, the polarizable force fields for acetone were proposed [25–27] whose creation was partly motivated by the behaviour of various acetone mixtures. For example, simulations of the acetone–water mixture displayed immiscibility throughout a range of acetone concentrations [8,28,29], which is not the case in reality. These findings hinted at the importance of refining the charge contributions in order to reproduce the mixing of acetone and water.

In this article, using molecular dynamics simulations, we are examining binary mixtures of acetone with pentane and carbon tetrachloride (CCl_4), as well as including some of the new results for benzene–acetone mixtures. Unlike benzene, which is a planar molecule, pentane is linear while carbon tetrachloride is globular (Figure 1). That way we can monitor the steric effects different shapes may have in mixtures with acetone. The chemical properties of the three non-polar molecules are similar [3], as is the way they are modelled [29,30]. To have the same conditions for all co-solvents, we used the point charged model for acetone as well [23,24]. Nonetheless, we

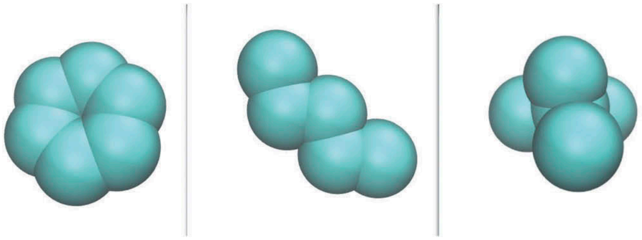

Figure 1. Models of solvent molecules: benzene (left), pentane (centre) and CCl_4 (right). The models are shown for illustrative purposes only, for their sizes are not depicted in proper proportions. The molar volumes of the molecules are $V_{BEN} = 89.2\,\frac{\text{cm}^3}{\text{mol}}$, $V_{PENT} = 115.3\,\frac{\text{cm}^3}{\text{mol}}$ and $V_{CCL} = 96.7\,\frac{\text{cm}^3}{\text{mol}}$.

modified the existing acetone model, for reasons which are discussed in the following sections. Finally, we present the new results for the acetone–methanol mixtures, which relate to the acetone structuring when mixed with molecules that have polar and non-polar constituents.

The rest of the paper is organised as follows. Section 2 gives the description of the theoretical and computational methods used in this work. Section 3 presents and discusses the various structural and thermodynamic results obtained, while Section 4 summarises the findings.

2. Materials and methods

2.1. *Theoretical details*

From the simulated data, we extracted the site–site correlation functions $g_{a_ib_j}(r)$, where a_i and b_j represent any two atomic sites on the molecules and i, j correspond to the species index, as the starting point for calculating other quantities. It is important to note that in the NpT ensemble, the correlation functions $g_{a_ib_j}(r)$ do not go strictly to unity (1) [31]. To remedy this problem, the tails of the correlation functions are shifted to the correct asymptote via the Lebowitz–Percus correction (LP) [32]. The procedure used is discussed in depth in previous papers [33].

A corrected $g_{a_ib_j}(r)$ is necessary to calculate the proper value of a quantity known as the Kirkwood–Buff integral (KBI) [34], which is defined as

$$G_{ij} = 4\pi \int \left[g_{a_ib_j}(r) - 1 \right] r^2 dr \tag{1}$$

where G_{ij} is the species or cross-species function. The Kirkwood–Buff (KB) theory of solutions defines the relationship between molecular distribution functions and thermodynamic quantities [34,35], thus becoming a bridge between the microstructure and macroscopic quantities. The KBIs for the two-component systems can be calculated using the thermodynamic approach [34,36,37]:

$$G_{ij} = \left[k_B T \kappa_T - \frac{\bar{V}_i \bar{V}_j}{VD} \right] (1 - \delta_{ij}) + \left[G_{12} + \frac{1}{x_i} \left(\frac{\bar{V}_j}{D} - V \right) \right] \delta_{ij} \tag{2}$$

where κ_T represents the isothermal compressibility (k_B is the Boltzmann constant and T is the temperature), $\bar{V}_i$ is the partial molar volume of species i, V is the total molar volume of the mixture and x_i is the mole fraction of species i. The D term is related to the chemical potential through the following expression [34,36,37]:

$$D = x_i \left(\frac{\partial \beta \mu_i}{\partial x_i} \right)_{TP} \tag{3}$$

where μ_i is the chemical potential of species i and $\beta = 1/k_B T$.

When several approximations are taken into account, Equation (2) can be reduced. The isothermal compressibility can be neglected since it is smaller in magnitude in comparison with other terms. Then, the partial molar volumes of the components can be replaced by the molar volumes of the neat components, thus ignoring the variations of excess volume. (The excess volume is at least one order of magnitude smaller than the volumes.) The D term depends on the chemical potential, which can be split into three different contributions (reference, ideal and excess parts): $\mu_i = \mu_i^{(0)} + k_B T \ln(\rho x_i) + \mu_i^{excess}$, and can be written as [36,37]

$$D = 1 + x_i \left(\frac{\partial \beta \mu_i^{excess}}{\partial x_i} \right)_{TP} \tag{4}$$

If we consider only the ideal part of the chemical potential and neglect the excess contribution, we would have $D = 1$. When $D = 1$ is inserted into Equation (2), one obtains the ideal KBIs. If we include the excess contribution of the chemical potential, the expression for D becomes more sophisticated and the KBIs start to deviate from ideality.

Another quantity calculated from site–site correlation functions $g_{a_ib_j}(r)$ is the site–site structure factor $S(k)$ [31]:

$$S_{a_ib_j}(k) = 1 + 4\pi\rho\sqrt{x_{a_i}x_{b_j}} \int \left[g_{a_ib_j}(r) - 1\right] \frac{sinkr}{kr} r^2 dr \tag{5}$$

where ρ is the total number density and x_{a_i} is the mole fraction of site a_i. The structure factors are Fourier transforms of the correlation functions $g_{a_ib_j}(r)$, as per standard numerical methods [38].

Site–site correlation functions $g_{a_ib_j}(r)$ are also used to calculate the site–site energy distributions in the form of running integrals [31]:

$$U_{a_ib_j}(r) = 2\pi\rho x_{a_i}x_{b_j} \int_0^r g_{a_ib_j}(r) v_{a_ib_j}(r) r^2 dr \tag{6}$$

where $v_{a_ib_j}(r)$ is the site–site interaction. This expression can be used to compute separately the running contributions from the site–site Lennard–Jones (LJ) interactions, as well as those from Coulomb interactions. By separating the two different contributions, one can gain more insight into the system's energetics in microscopic terms and how the different contributions shape the macroscopic energy. In the calculation of the Coulomb energy, it is more convenient to use the term $g(r) - 1$. Because of the overall electroneutrality of the system, the additions of 1 do not influence the final result. However, due to this transformation, the energy distributions of the same charges are negative, while the opposite-charged energy distributions are positive.

The pair correlations can be also utilised to calculate the excess two-particle entropy. The expression for the entropy in terms of the expansion of the one-body, two-body, etc. contributions was defined in [39] and separately [40] and further adapted by Baranyai and Evans [41]. This modification concerns the introduction of a local expression for entropy, which is ensemble invariant, similar as in the case of the modification applied to the Coulomb energy distribution. The equations for mixture were proposed by Laird et al. [42]. This method was applied to calculations of the entropy in liquid water [43,44], solvation energies [45,46] and description of the hydrophobicity [47]. Here we used a simplified expression for the molecular liquids, which excludes the angular dependence in two-body term as reported in [48]:

$$S^{excess} = -2\pi k_B\rho \sum_{a_ib_j} x_{a_i}x_{b_j} \int \left(g_{a_ib_j} \cdot lng_{a_ib_j} - g_{a_ib_j} + 1\right) r^2 dr \tag{7}$$

2.2. *Simulation details*

Molecular dynamics simulations were conducted in the Gromacs program package [49]. Packmol [50] was used for creating initial configurations for all systems. The simulations were done in the NpT ensemble at ambient conditions ($T = 300K$, $p = 10^5 bar$), utilising the Parrinello–Rahman barostat [51,52] and v-rescale thermostat [53]. The long-range electrostatics were handled with particle mesh Ewald technique [54]. The simulation protocol was the same for all systems. Following the energy minimisation, equilibration runs were performed, followed by production runs. For neat systems, equilibration lasted typically 1 ns and production 3 ns. In the case of mixtures, both the equilibration and production runs lasted for 5 ns.

We tested several models for pure acetone: the classic united atom OPLS [23] and TraPPe [24] force fields, alongside a modified OPLS force field. The latter combined the partial charges parametrised for the all atom OPLS ketone model [55] with the united atom representations of the methyl groups [29]. In brief, the major difference between the classic OPLS-UA model and our modified OPLS-UA model is the distribution of partial charges on the sites, as can be ascertained from Table 1. The rationale for modifying the existing OPLS-UA model is explained in Section 3.1, where the results for neat acetone are disseminated.

As for the non-polar solutes, benzene and pentane were modelled with the OPLS-UA force field [29], while the OPLS-AA model was used for carbon tetrachloride [30]. Additionally, the TraPPe-UA model of benzene was taken into consideration [56], in order to test the mixture with its complementary TraPPe acetone. In the case of methanol, the OPLS-UA model was used [57].

The system sizes of pure liquids were either 1000 or 2000 molecules. For neat acetone, 1000 molecules were used for the classic OPLS-UA force field and 2000 molecules for the other two force fields tested. The neat non-polar solutes contained 1000 molecules each, while neat methanol had 2000 molecules.

Binary mixtures typically contained 2000 molecules and were simulated for three molar fractions of acetone: 0.2, 0.5 and 0.8. A simulation of acetone–pentane containing 16,000 particles was performed for the molar fraction $x_{\mathrm{ACE}} = 0.2$ to check whether or not the system size plays a role in obtaining a good convergence of the tail of the pair correlation functions. The results for both big and small system were nearly identical, as represented in some of the results. Also, a 16k system of the acetone–methanol mixture was simulated for the $x_{\mathrm{ACE}} = 0.8$ mol fraction, and the difference between 2k and 16k systems is discussed.

Cluster size distribution probabilities were calculated with the Gromacs module *g_clustsize*. The calculations are done taking into account the geometric criteria, where the choice of the cut-off distance defines if two sites participate in a cluster. Usually, the cut-off falls close to the first minimum of the pair correlation function. In the case of acetone and different solute molecules, the sites selected for analysis were carbon atoms, and the values were $r_{cutoff} = 7.0\mathring{A}$.

3. Results and discussion

3.1. *Neat acetone*

Table 2 summarises the calculated thermodynamic properties – density and heat of vaporisation – for the simulated acetone models, comparing them with their respective experimental values [58]. At a glance, the TraPPe-UA acetone performs the best, being in the 3% deviation density-wise and within per cent deviations of 2% for the enthalpy of vaporisation (H_{VAP}). The classic OPLS-UA follows close

Table 1. Parameters used for all modelled liquids.

Acetone model	Site	q [e]	σ [Å]	ε [kJ/mol]
OPLS-UA [23]	C	0.300	3.750	0.439
	O	−0.424	2.960	0.879
	M	0.062	3.910	0.670
TraPPe-UA [24]	C	0.424	3.820	0.332
	O	−0.424	3.050	0.657
	M	0.0	3.750	0.814
Modified OPLS-UA [55]	C	0.470	3.750	0.439
	O	−0.470	2.960	0.879
	M	0.0	3.775	0.866
Solute model	Site	q [e]	σ [Å]	ε [kJ/mol]
CCl_4 [30]	C	0.248	3.8	0.209
	Cl	−0.062	3.47	1.113
Pentane [29]	CH_3	0.0	3.905	0.732
	CH_2	0.0	3.905	0.494
Benzene – OPLS UA [29]	CH	0.0	3.75	0.460
Benzene – TraPPe UA [56]	CH	0.0	3.695	0.420

The first part of the table is designated for tested acetone models. The sites are: C – central carbon atom; O – oxygen atom; M – methyl group united atom. The second part of the table contains the parameters for the solutes: CCl_4, pentane and benzene.

Table 2. Thermodynamic results for tested acetone models.

Model	Density [kg/m^3]	H_{VAP} [kJ/mol]
Modified OPLS-UA	818.5 (±3.3)	33.3 (±0.16)
OPLS-UA	738.8 (±5.1)	18.0 (±0.11)
TraPPe-UA	761.6 (±4.1)	31.7 (±0.17)
Experiment [58]	784.5	30.99

behind in terms of density, being at 6% deviations from the experimental value, but significantly underestimating the value of H_{VAP} with a 40% deviation from the experimental value. The latter fact was the main reason the modification of the OPLS model was undertaken. The modified OPLS acetone yielded a density within 4% deviations, and an H_{VAP} within 7% of the experimental value, which places it above the classic OPLS-UA acetone in terms of accuracy.

Figure S1 contains the relevant pair correlation functions for all three models: the radial distribution functions (RDFs) of acetone's central carbon atom in the main panel and the RDFs of the methyl groups in the inset. The RDFs in the main panel show significant overlap, with the only difference being the slight shift to the left in the second neighbour shell for the modified OPLS-UA model. The RDFs of the methyl groups have a double-peak feature in the first neighbour shell, coming from the fact that the acetone molecule has two methyl groups flanking the central carbon atom. The first small peak, located at ~4 Å, differs in height from one model to another, but from that position onward, the RDFs are identical for all the models. Moreover, the structural results are in line with the results obtained from other simulation [59,60] and experimental studies [61].

When all of these findings are taken into account, we can conclude that all of the tested models perform reasonably well and will suit the purposes of a structural study. However, since the TraPPe force field does not model carbon tetrachloride, we chose to perform the bulk of the simulations in the modified OPLS force field for the sake of consistency.

3.2. *Mixtures with acetone as the common solvent*

3.2.1. *Snapshots*

Figure 2 shows one configuration of the acetone–pentane system for the three concentrations studied. Pentane molecules are coloured in transparent grey, in order to see more clearly the structuring of the acetone molecules.

At the highest acetone mole fraction, x_{ACE} = 0.8 (left panel of Figure 2), we notice patches of pentane amidst the acetone molecules. As acetone is rarified (visible for x_{ACE} = 0.5 and especially x_{ACE} = 0.2, the middle and right panel of Figure 2), dimers and short chains are more noticeable.

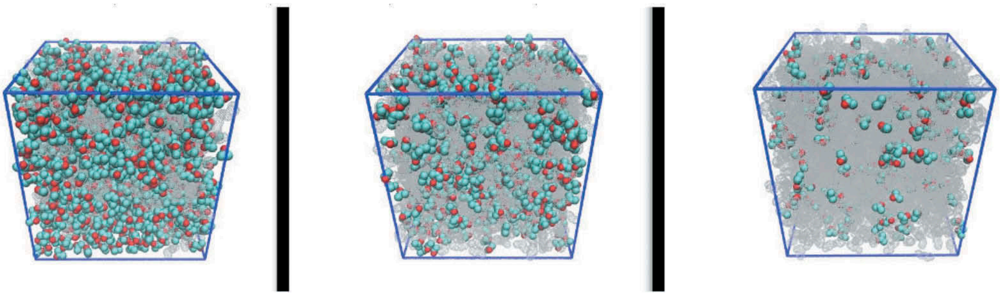

Figure 2. Snapshot of the acetone–pentane mixture for the following molar fractions of acetone: 0.8 (left), 0.5 (middle) and 0.2 (right panel). The pentane molecules are represented in transparent grey, while acetone molecules are presented in cyan (carbon atoms) and red (oxygen atom).

However, the snapshots are used solely for illustrative purposes, since they show only one realisation of the system.

3.2.2. *Cluster distribution probabilities*

In Figure 3, we show the cluster distribution probabilities for all three acetone mixtures: acetone–CCl_4 (left panel), acetone–pentane (middle panel) and acetone–benzene (right panel), for the three typical acetone concentrations (0.2 – blue, 0.5 – green and 0.8 – magenta). The upper panels contain the cluster distribution probabilities computed for acetone's central carbon atom. In the lower panel, we show the cluster probabilities of certain carbon atoms belonging to each solute.

The cluster calculation results reveal that both species, regardless of the mixture, follow the tendencies seen in LJ mixtures [62,63]. At low concentrations, the cluster distribution is a monotonously decaying function, illustrating that monomers are the likeliest to be found in the mixture. As the concentration of the species increases, the distribution will gain a new peak, occurring at very high cluster sizes. This indicates the heightened probability of big, system-size clusters – an expected consequence of the species being in the majority in a case of simple solutions.

The acetone's cluster distributions, regardless of the mixture, follow this general pattern. The cluster analysis of the solutes reveals some interesting details. With the change in concentration, the cluster distributions of CCl_4 and benzene are practically interchangeable. The behaviour of pentane has a slightly different pattern. Although pentane forms system-size aggregates at x_{ACE} = 0.2, the likelihood of their occurrence is lower than in the case of benzene or CCl_4. At $x_{ACE} = 0.5$ and 0.8, the biggest clusters pentane may form are noticeably smaller than those formed by CCl_4 and benzene. When a mixture is dominated by a solvent with energetic interactions, the solute molecules will be able to aggregate in bigger groups if their shape is more compact. Pentane, being chain-like, is more likely to be thwarted in its aggregation than its planar or globular counterpart.

Finally, the clusters mentioned in context of acetone mixtures are weaker and formations more transient, comparing to the clusters in neat alcohols or mixtures of alcohols and non-polar solutes [64,65], which renders them less detectable by this type of analysis.

3.2.3. *Pair correlation functions*

Figure 4 shows the pair correlation functions for the three acetone mixtures, organised as in Figure 3. The results for the equimolar mixture of acetone and benzene were already shown in a previous work [19], but are included here for comparison. The upper panel is reserved for the *g*

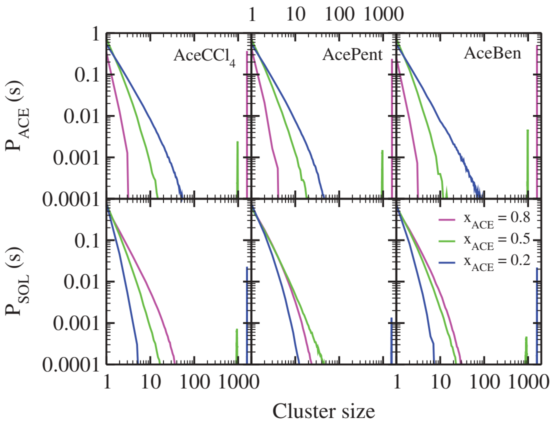

Figure 3. Cluster distribution probabilities for the mixtures of: acetone–carbon tetrachloride (left), acetone–pentane (middle) and acetone–benzene (right panel). The results are shown for three acetone mole fractions: 0.2 (blue), 0.5 (green) and 0.8 (magenta). The probabilities for the central acetone carbon are presented in the upper row, while the lower row contains the results for the designated carbon atom of the solute (see text).

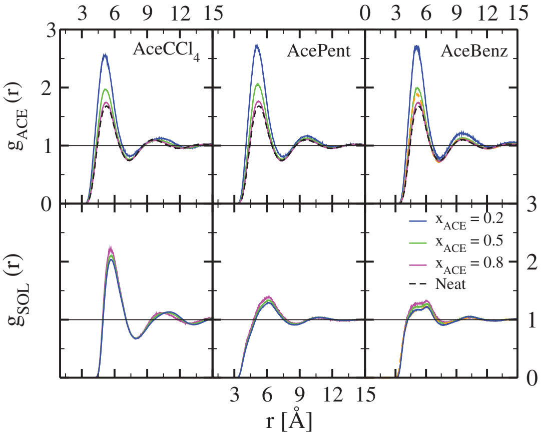

Figure 4. Pair correlations functions for: acetone–CCl$_4$ (left), acetone–pentane (middle) and acetone–benzene (right panel) for three typical concentrations (the colour code is in the legend). The correlation functions for the central acetone carbon are presented in the upper row, while the lower row contains the results for the designated carbon atom of the solute (see text). The dashed orange line in the panels designated for the acetone–benzene mixture corresponds to results obtained with the TraPPe force field for both acetone and benzene.

$(r)s$ of the central acetone atom, while the lower panel shows the $g(r)s$ of the same solute carbon atoms as in Figure 3.

The acetone correlation functions for all three mixtures are almost indistinguishable, indicating that, in terms of short-range structuring, acetone behaves exactly the same in every non-polar solute. The correlation functions of neat acetone and acetone at $x_{\mathrm{ACE}} = 0.8$ mol fraction are nearly the same, but as the acetone content is decreased, the first peak, located at $r = 6Å$, noticeably increases.

This behaviour contrasts that of the carbon atoms of the various solutes. Whether benzene, pentane or CCl$_4$ are in question, the heights of their first peaks change very little with the change in concentration. The correlation function of CCl$_4$ resembles more the correlations of the LJ atoms [66] than benzene or pentane, which is due to the close packing enabled by the molecular shape. However, the general trend of solutes' correlation functions is akin to that observed in the benzene–pentane system [19], which is an example of simple disorder.

The change in the cross correlation functions of all three systems is negligible with the change of mole fraction (Figure S3), which indicates that acetone molecules have the same preference for the solute molecules, regardless of the concentration. That, in turn, means that acetone's interactions are the ones driving the acetone grouping as acetone molecules grow scarcer.

To close this subsection, we observe that the correlation functions of acetone and benzene, calculated for the TraPPe models for $x_{\mathrm{ACE}} = 0.5$ (orange dashes, right panels of Figure 4 and S3), lie closely together to the OPLS data.

3.2.4. *Structure factors*

To extract information about the long-range structuring, we turn to the site–site structure factor analysis, showcased in Figure 5. The structure factors are calculated from the correlation functions presented in Figure 4, and organised by mixture and species in the exact same order. At first glance, the behaviour of acetone is almost identical in all three mixtures. The only prominent feature in the structure factors is the main peak, situated at $k = 1.4Å^{-1}$, which approximately corresponds the size of the site ($r = \frac{2\pi}{k}$). Just like in Figure 4, where the acetone's correlations functions nearly overlapped, acetone's structure factors show the same position and height of the main peak, and a significant raise at $k = 0$. As acetone is rarified, the main peak decreases, and the raise at $k = 0$ increases for all systems. This raise at $k = 0$

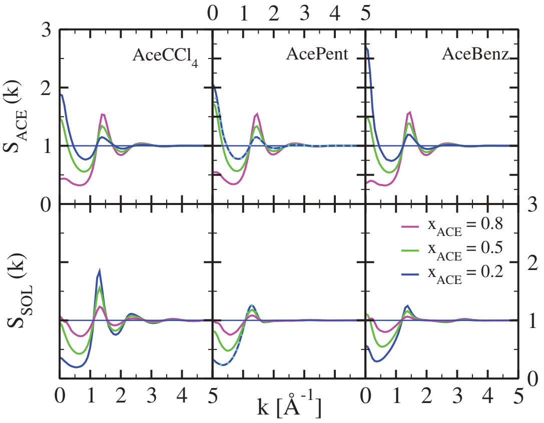

Figure 5. Structure factors calculated from the pair correlation functions in 4. The figure has the same layout as 4; acetone–CCl_4 (left), acetone–pentane (middle) and acetone-benzene (right panel) structure factors are shown for three typical concentrations (the colour code is in the legend). The structure factors for the central acetone carbon are presented in the upper row, while the lower row contains the results for the designated carbon atom of the solute (see text). The dotted turquoise lines in the middle panels represent the results obtained from the simulation of acetone-pentane, system size 16k, for $x_{ACE} = 0.2$.

points at the enhanced concentration fluctuations acetone exhibits not only in benzene [19] but also in the other two compounds.

It is known that neat systems which exhibit clustering, such as alcohols, will invariantly show a signature of those objects in the appropriate site–site structure factors – the so-called pre-preak, located at small k values [67,68]. Similarly, in some of the binary mixtures, such as benzene–alcohol or water–alcohol mixtures, with at least one associating species, the self-segregations or formation of the micro-heterogeneous domains, is observed through pre-peaks et even smaller k values [20].

In the cases of acetone shown above, we lack a pre-peak in the small k region of the structure factor, which hints that there are no micro-heterogeneous domains formed in this system. What we detect through the site–site structure factor analysis are solely concentration fluctuations. Granted, there are small variations in the concentration fluctuations, depending on the solute, which are most visible for the $x_{ACE} = 0.2$ mol fraction, but the overall effect is very similar, regardless of the solute.

Possible origin of the enhanced concentration fluctuations may come from the local energetic frustration that acetone's molecules experience. In the neat liquid, acetone molecules can freely arrange themselves, forming energetically favourable dimers or larger structural associations. The addition of bulky solute molecules will prevent acetone molecules from achieving preferential correlations as in the neat liquid, therefore leading to a frustrated system which will have the side effect of heightened concentration fluctuations. This is the most apparent for the $x_{ACE} = 0.2$ mol fraction.

As for non-polar solutes (lower panel of Figure 5), all of them possess their characteristic main peak, positioned at $k = 1.25\mathring{A}^{-1}$. That main peak in the $S(k)$ is of the same height for benzene and pentane, and somewhat higher for CCl_4. The structure factors for all three solvents also show a raise at $k = 0$, which is significantly smaller than in the case of acetone. That implies that acetone is the one driving the structuring in all of these mixtures, and that the characteristics of the non-polar solutes will not have a great influence on the ordering.

On a different note, additional structure factors for acetone and pentane, obtained from simulations of a 16k system for the lowest acetone molar fraction, are added in dots to the middle panels of Figure 5. Since those results are practically interchangeable with the results for the 2k system, we can conclude that the smaller system is sufficient to reproduce the correct long-range structuring in these mixtures, as observed in simulation studies.

3.2.5. *KB integrals*

Figure 6 contains KBIs over molar fraction of solvent for both acetone–pentane (left panel) and acetone–CCl_4 (right panel). Both mixtures exhibit a weak nonideality in terms of KBI. The D function, shown in the inset of Figure 6, yields GAB which match the trend of the simulated KBIs. The fitted D has a form $D(x) = 1 - \alpha x(1 - x)$, where $\alpha = 2$. The same function was previously used for the case of benzene–acetone mixtures [19]. The discrepancies between the calculated KBIs and the ones obtained from the simulation (especially in the case of CCl_4 in the right panel) may result from the fact that the simulated pure liquids (acetone and CCl_4) do not have the exact volume of the real systems.

Furthermore, when comparing the KBIs from Figure 6 to those presented in our previous work on acetone–benzene [19], we see the similarity between all three acetone binary mixtures. Despite the difference between the solvents in terms of geometry, the concentration fluctuations present in the systems are startlingly similar, not only for acetone but also for the non-polar solvent. However, the shape of the D and, consequentially, the shapes of the KBI curves, reveal a system that is neither ideal (dashed lines in Figure 6) nor similar to the micro-heterogeneous system [69,70]. That only confirms the picture that acetone mixtures are entrenched between simple and complex mixtures.

3.2.6. *Energy distributions*

Now we turn to the analysis of the energy distributions in the systems. The results for neat acetone were presented to some extent in a previous work [71], so we have included all possible site–site contributions in the Supplementary material, Figure S2. For the neat liquid, all site–site van der Waals distributions follow the same trend, converging to their proper values after 15 Å. However, the Coulomb running energies show oscillations which extend beyond and are also reflected in their sum. The totals of both running energies correspond to the respective average

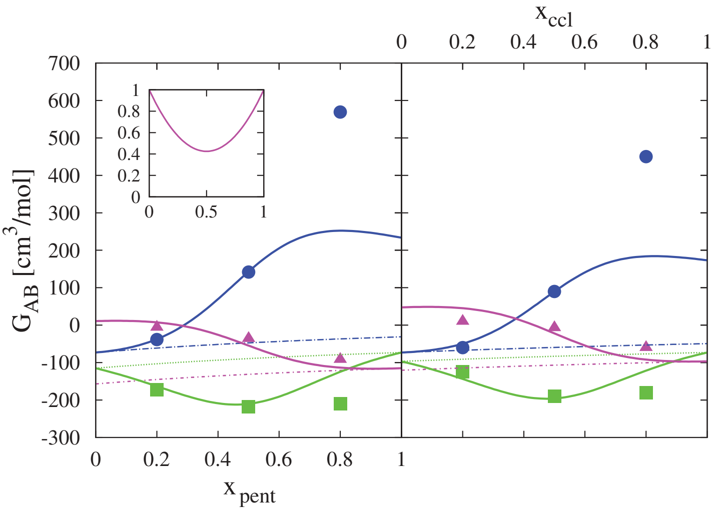

Figure 6. Kirkwood–Buff integrals of the acetone–pentane (left panel) and acetone–carbon tetrachloride (right panel) mixtures. Colour code is as follows: blue is for acetone–acetone, magenta is for solute–solute and green for the cross KBI. Symbols correspond to KBIs from present simulations, dashed lines represent ideal KBI, while full lines correspond to the KBI calculated with nonideal D (in the inset).

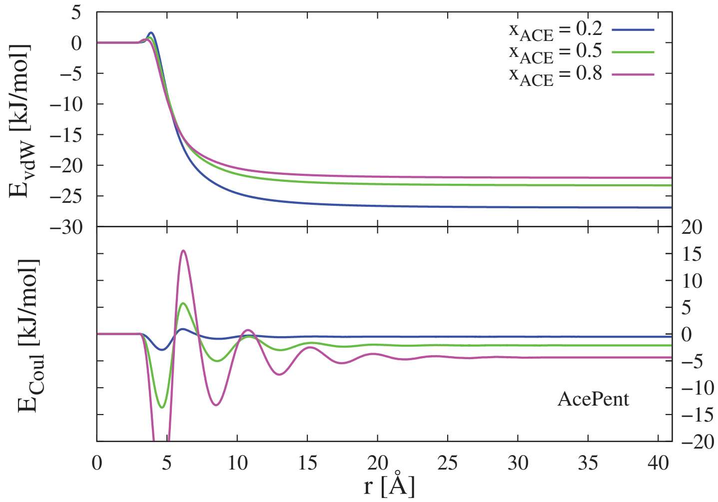

Figure 7. Energy distributions of the acetone–pentane system, split into van der Waals contributions (upper panel) and Coulomb contributions (lower panel). The data are shown for three different molar fractions of acetone, with the colour code in the legend.

values obtained from the simulation, which are around −25 kJ/mol for van der Waals and −7 kJ/mol for Coulomb contributions.

Figure 7 shows the energy distributions of the acetone–pentane mixtures at three different acetone concentrations, split into the total van der Waals contribution (upper panel) and total Coulomb contribution (lower panel). As we can see, the running van der Waals energies for the mixtures follow the trivial behaviour seen in neat liquids, but the values vary depending on the molar fraction of acetone. This is also true in the cases of the acetone–benzene and acetone–CCl_4 mixtures (Figure S4).

The total running Coulomb energies for all concentrations resemble that of neat acetone – oscillatory functions which converge to the average value calculated from the simulation. However, a fuller insight into the energetics of the mixture comes from examining the individual site–site contributions, which are shown in Figure 8 for all three molar fractions of acetone. At $x_{\mathrm{ACE}} = 0.8$ (lower panel of Figure 8), all the site–site running Coulomb energies follow the trends set by their counterparts in neat acetone (Figure S2). As acetone is rarified, we witness interesting new features emerging in the site–site running energies. At $x_{\mathrm{ACE}} = 0.5$, all three site–site contributions have a modulation in the tail of the function, stemming from a long-range modulation present in the acetone's $g(r)$. This is further enhanced for $x_{\mathrm{ACE}} = 0.2$. Once again, these features occur in the other two acetone–non-polar solute mixtures (Figure S5).

It is important to note that, despite the site–site running Coulomb energies individually displaying such an interesting feature, the modulations cancel themselves when superimposed, resulting in the total running Coulomb energy resembling that of neat acetone. This example illustrates how site–site functions may have noteworthy properties (signatures), which can be completely suppressed when considering their sum.

One may also debate how the LP correction, employed in the treatment of the pair correlation function to obtain the asymptote of 1, will affect the site–site running Coulomb energies. As witnessed in Figure S6, the running energies calculated from untreated $g(r)$s show a more pronounced modulation in the long range. However, the LP correction cannot erase the modulation in the tail of the $g(r)$ (Figure S6 inset), which confirms that it is a signature of the specific underlying structuring.

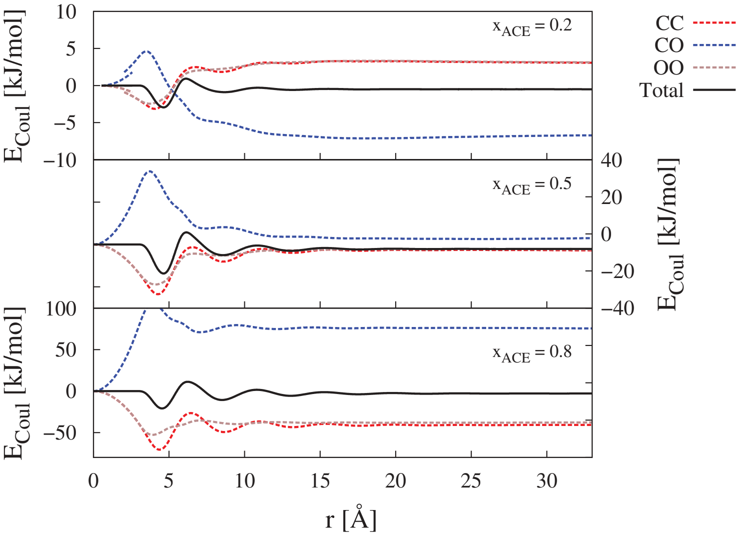

Figure 8. Site–site Coulomb energy distributions for the acetone–pentane mixture, $x_{ACE} = 0.2$ (upper panel), 0.5 (middle panel) and 0.8 (lower panel). The colours corresponding to the site–site distributions and their total are contained in the legend.

3.2.7. *The case of the acetone–methanol mixture*

Given that this work focuses on acetone mixtures, another system with acetone as the solvent is worth mentioning: acetone–methanol. The structural complexity of the system was already noted by some of the authors [72,73].

To illustrate this point, we turn to Figure 9, where the site–site correlation functions and structure factors for three different concentrations of acetone are shown. In this case, it is noticeable that the correlation functions of acetone's carbon change very little with the change in concentration. This is at variance with methanol's OO and CC correlations, which increase with the decrease in methanol mole fraction. In terms of short-range organisation, acetone

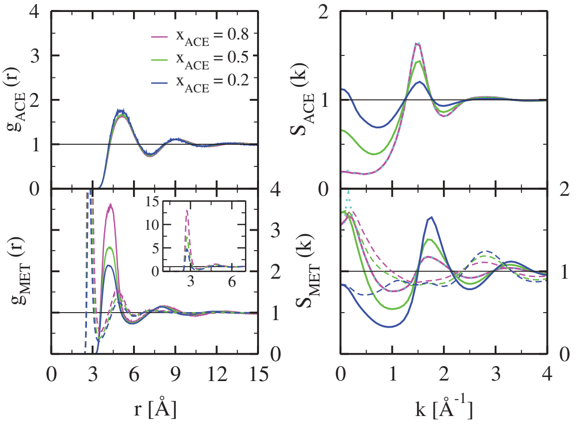

Figure 9. Site–site correlation functions (left panel) and structure factors (right panel) for the acetone–methanol mixture, according to the molar fraction of acetone (colour code in the legend). The top row contains the correlation functions and structure factors of the main carbon atom in acetone; the lower row contains same quantities for methanol's carbon atom (full lines) and oxygen atom (dashed line). The inset in the lower left panel shows the full range of OO methanol correlations. The dotted turquoise lines in the structure factor panels represent results for the 16k system, $x_{ACE} = 0.8$.

follows the pattern of non-polar solutes from acetone–non-polar solutes mixtures, while methanol is the one driving the structural organisation. The structure factor analysis also points in that direction – as acetone gets scarcer, its structure factors show more concentration fluctuations, but not as much as in a non-polar, charge-less environment. In fact, acetone's structure factors vary with concentration just like the non-polar solutes' structure factors in Section 3.2.4. Methanol, on the other hand, displays a clear signature of a cluster peak in its OO structure factor for $x_{\mathrm{ACE}} = 0.2$, similar to the one in neat methanol [67,68]. As more acetone is added, methanol's structure factors broaden, which might be an indication of the domains formed by the methanol clusters. This goes to show that the species which has the stronger electrostatic interaction – in this case methanol with its hydrogen bond – will take over the role of the main structuring agent, while the other component will be forced to adapt to the structuring enforced by the more charged species. Figure 9 also shows the comparison of the site–site structure factors for the 2k and 16k system, for $x_{\mathrm{ACE}} = 0.8$. For this mole fraction, the structure factors of acetone are the same, regardless of the system size, while for the structure factors of methanol the effects of the finite size system are observed – the small k behaviour is not the same for the 2k and 16k system.

The site–site running Coulomb energies (Figure 10) are shown for selected site–site combinations for both methanol and acetone. In this example, methanol's running Coulomb energies display a slight modulation in the long-range part of the distribution for $x_{\mathrm{ACE}} = 0.8$ and 0.5 concentrations (perhaps rendered less visible because of the range in the lowest panel of Figure 10). Acetone, on the other hand, shows the same behaviour as in neat acetone, meaning purely oscillatory functions without any kind of modulation in the long-range part.

3.2.8. *Excess thermodynamic quantities*

Figure 11 displays the results of excess enthalpies and excess pair entropies for all the studied acetone mixtures. The acetone–non-polar solute systems are grouped together in the left panels, while the acetone–methanol results are presented in the right panels.

The excess enthalpies (upper row in Figure 11) are positive for all studied systems. Positive excess enthalpy signifies a positive energetic contribution to the Gibbs free energy, which in turn

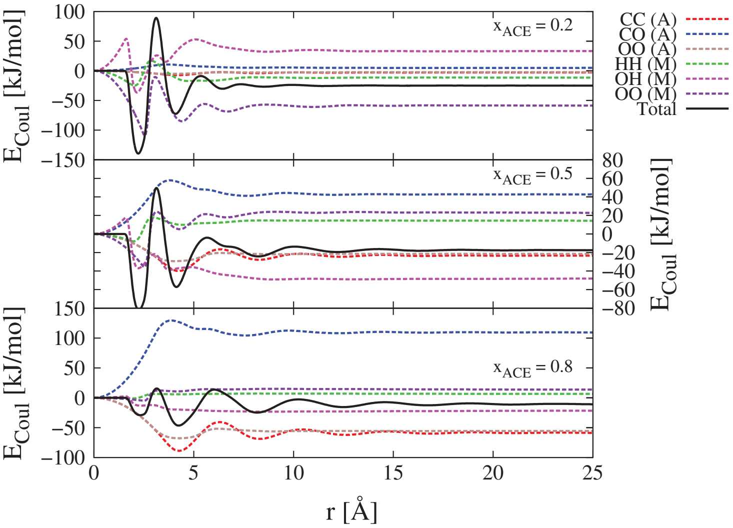

Figure 10. Selected site–site Coulomb energy distributions for the following mole fractions of the acetone–methanol mixture: $x_{\mathrm{ACE}} = 0.2$ (upper panel), $x_{\mathrm{ACE}} = 0.5$ (middle panel) and $x_{\mathrm{ACE}} = 0.8$ (lower panel). The colours corresponding to the selected site–site distributions and the total of all contributions are contained in the legend.

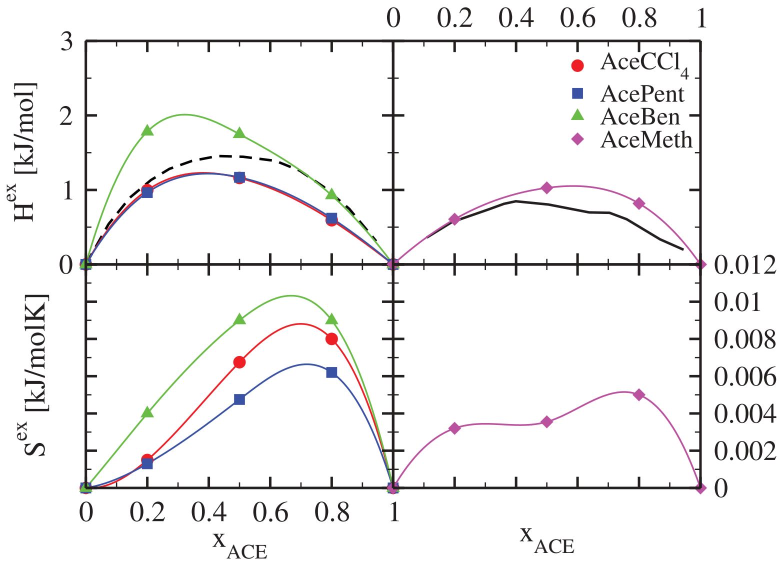

Figure 11. Excess enthalpies (upper row) and excess entropies (lower row) for acetone–non-polar solute (left panels) and acetone–methanol (right panels). The colour code for each mixture is contained in the legend. The dashed black and the full black lines are the experimental excess enthalpies for acetone–pentane [74] and acetone–methanol [75].

means that mixing acetone with these other solutes is not an energetically favourable process. This trend is the same as in realistic systems, as evidenced by the experimental results for acetone–pentane [74] and acetone–methanol [75] mixtures. Furthermore, the calculated excess enthalpies for acetone–pentane and acetone–methanol correspond fairly well to the experimental values, indicating that the models qualitatively reproduce the energetics of these systems.

The excess entropies (lower row in Figure 11) are also positive for all systems. The positive calculated excess values contribute to the lowering of the Gibbs free energy, rendering the process of mixing acetone with all the other solutes entropically favourable (although we present only a part of the total entropy of mixing).

In the case of acetone-non-polar solutes, the trend of the excess pair entropy is similar for all three systems. The values tend to peak for the systems at $x_{\mathrm{ACE}} = 0.8$ mol fraction, decreasing as acetone is rarified. The smaller entropic contribution at low mole fractions of acetone points to less favourable mixing, which goes in line with the observed heightened concentration fluctuations occurring at $x_{\mathrm{ACE}} = 0.2$.

As for the acetone–methanol mixture, its excess entropy curve varies strongly with concentration exhibiting a very complex shape. It is smaller than the excess entropy for non-polar–acetone mixtures, with the maximum at the $x_{\mathrm{ACE}} = 0.8$ mol fraction, decreasing as the number of acetone molecules is decreasing.

We may give a tentative explanation, keeping in mind that the used definition of the excess two-particle entropy is too simple, especially when applied to the associated system [47]. When methanol is in the majority, formations of the hydrogen-bonded clusters reduce the overall entropy of mixing. The menthol clusters persist, even when adding more acetone, favouring the lower entropy. We may also introduce the idea from Kollipost et al. [9] that acetone dislikes to associate with the hydrogen-bonded clusters. Therefore, both species are constrained, methanol due to the hydrogen-bonding and acetone due to the excluded volume taken up by the methanol clusters. This effect might be most noticeable at the middle of the concentration range and may explain why the excess entropy at the $x_{\mathrm{ACE}} = 0.5$ mol fraction is comparable to the one at the $x_{\mathrm{ACE}} = 0.2$. As we increase the concentration of acetone even more, the contribution of the methanol clusters decreases and acetone molecules are less constrained which causes the excess entropy to rise, increasing the favourability of the mixing process.

4. Conclusions

In this work, we studied binary mixtures of acetone with non-polar solutes of different molecular topology. We used a modified force field for acetone based on the OPLS-UA model [23,55]. Focusing on mainly static properties, we aimed to describe the observed structuring which is in between simple and complex liquids.

The structural properties of acetone, coupled with the KBIs, showed extreme similarities in all three investigated mixtures. Furthermore, acetone's behaviour illustrates the main signatures of the weak local ordering which its interactions produce. In terms of the pair correlation functions, there is a noticeable increase of the first peak as acetone is rarified. As for site–site structure factors, they lacked evidence of structuring at small k values, yet pointed to appreciable concentration fluctuations at small molar fractions of acetone. The latter was also confirmed by the KBIs. The energy distribution results underline the weak local ordering picture, with the running Coulomb energies pointing to the fact that acetone is driving the structural and energetic behaviour of these mixtures.

We also uncover the effects of solute shape on the disorder generated by acetone's dipolar interactions. The solutes only show subtle differences in the properties investigated; most noticeably in the first neighbours of the pair correlation function and the cluster probability distributions. However, as a whole, the analysed quantities witnessed the same general trends for all three solutes; therefore, the molecular shape of the solutes does not affect the long-range structuring.

All of those features confirm the existence of a weak nonideality in these systems, which is dictated by the acetone's interactions. To contrast these findings, we included key results of a known complex mixture, acetone–methanol, such as the strong concentration variation of the correlation functions and the signature of the micro-heterogeneous domains in site–site structure factors at the small k vector. In this mixture, methanol is the component which enforces its own structuring while acetone adapts to these conditions.

Finally, we analysed the excess thermodynamic properties of all four mixtures. In all cases, the excess enthalpies and excess entropies were positive, illustrating the fine balance between energetic and entropic contributions which governs the mixing process. The molecular insight provided in this study might be a starting point for understanding solvation processes relevant for various application purposes. For example, acetone–non-polar solvent mixtures are featured prominently in compound extraction, especially where the compounds have a wide range of polar and non-polar constituent groups, such as carotenoids [76]. Therefore, the weak nonideality could be a beneficial feature when considering the solubility of complex components.

Acknowledgments

The authors would like to thank the Croatian Science Foundation (Installation Research Project UIP-11-2013-4514 'Multi-scale description of meso-scale domain formation and destruction') for their financial support. MP thanks L'Oréal ADRIA d.o.o. together with the Croatian jury for UNESCO for the grant "For Women in Science". Also, the authors acknowledge the support of Franjo Sokolić, Aurélien Perera, Bernarda Lovrinčević and Tomislav Primorac.

Disclosure statement

No potential conflict of interest was reported by the authors.

Funding

The authors would like to thank the Croatian Science Foundation (Installation Research Project UIP-11-2013-4514 ‘Multi-scale description of meso-scale domain formation and destruction’) for their financial support. MP thanks L’Oréal ADRIA d.o.o. together with the Croatian jury for UNESCO for the grant “For Women in Science”.

ORCID

Martina Požar http://orcid.org/0000-0001-6300-2204

References

[1] Remler RF. The solvent properties of acetone. Ind Eng Chem. 1923;15:717–720.
[2] Kostag M, Liebert T, Heinze T. Acetone-based cellulose solvent. Macromol Rapid Comm. 2014;35:1419–1422.
[3] Orchin M, Macomber R, Pinhas A, et al. The vocabulary and concepts of organic chemistry. 2nd ed. Hoboken (NJ): John Wiley & Sons; 2005.
[4] McLain S, Soper A, Luzar A. Orientational correlations in liquid acetone and dimethyl sulfoxide: a comparative study. J Chem Phys. 2006;124:074502.
[5] Saito H, Tanaka Y, Nagata S, et al. ^{13}C nuclear magnetic resonance studies on molecular association. I. Self-association of dipolar molecules. Can J Chem. 1973;51:2118.
[6] Ancian B, Tiffon B, Dubois JE. Molecular interactions and reorientational motion of neat acetone in the liquid state. ^{17}O NMR chemical shifts and linewidths at variable temperature. Chem Phys. 1983;74:171.
[7] Idrissi A, Polok K, Barj M, et al. Free energy of mixing of acetone and methanol: a computer simulation investigation. J Phys Chem B. 2013;117:16157–16164.
[8] Jedlovszky P, Idrissi A, Jancsó G. Can existing models qualitatively describe the mixing behavior of acetone with water? J Chem Phys. 2009;130:124516.
[9] Kollipost F, Domanskaya A, Suhm M. Microscopic roots of alcohol-ketone demixing: infrared spectroscopy of methanol-acetone clusters. J Phys Chem A. 2015;119:2225–2232.
[10] Musso M, Giorgini M, Doge G, et al. The non-coincidence effect in highly diluted acetone-ccl I. Experimental results and theoretical predictions 4 binary mixtures. Mol Phys. 1997;92:97.
[11] Torii H, Musso M, Giorgini M, et al. The non-coincidence effect in highly diluted acetone-CCl4 binary mixtures II. Experimental, theoretical and monte carlo simulation results. Mol Phys. 1998;94:821.
[12] Musso M, Giorgini M, Torii H, et al. The Raman non-coincidence effect of the ^{12}CO stretching mode of liquid acetone in chemical and in isotopic mixtures. J Mol Liq. 2006;125:115.
[13] Arivazhagan G, Elangovan A, Shanmugam R, et al. Spectroscopic studies, nbo analysis and dielectric studies on the behaviour of acetone molecules in non-polar solvent environment. Chem Phys Lett. 2015;627:101.
[14] Jalilian M. Spectra and structure of binary azeotropes: IV. Acetone-cyclohexane. Spectrochim Acta A. 2008;69:812.
[15] Shikata T, Sugimoto N. Dimeric molecular association of dimethyl sulfoxide in solutions of nonpolar liquids. J Phys Chem A. 2012;116:990.
[16] Anderson D, Hall J, Babb A. Mutual diffusion in non-ideal binary liquid mixtures. J Phys Chem. 1958;62:404–408.
[17] Burchard J, Toor H. Diffusion in an ideal mixture of three completely miscible non-electrolytic liquids - toluene, chlorobenzene, bromobenzene. J Phys Chem. 1962;66:2015–2022.
[18] Janzen T, Gaponenko Y, Mialdun A, et al. The effect of alcohols as the third component on diffusion in mixtures of aromatics and ketones. RSC Adv. 2018;8:10017–10022.
[19] Požar M, Seguier JB, Guerche J, et al. Simple and complex disorder in binary mixtures with benzene as a common solvent. Phys Chem Chem Phys. 2015;17:9885.
[20] Požar M, Lovrinčević B, Zoranić L, et al. Micro-heterogeneity versus clustering in binary mixtures of ethanol with water or alkanes. Phys Chem Chem Phys. 2016;18:23971.
[21] Dixit S, Crain J, Poon W, et al. Molecular segregation observed in a concentrated alcohol-water solution. Nature. 2002;416:829–832.
[22] Guo JH, Luo Y, Augustsson A, et al. Molecular structure of alcohol-water mixtures. Phys Rev Lett. 2003;91:157401.
[23] Jorgensen W, Briggs J, Contreras M. Relative partition coefficients for organic solutes from fluid simulations. J Phys Chem. 1990;94:1683.
[24] Stubbs J, Potoff J, Siepmann J. Transferable potentials for phase equilibria. 6. United-atom description for ethers, glycols, ketones, and aldehydes. J Phys Chem B. 2004;108:17596.
[25] Rusu V, Bachmann S, van Gunsteren W. Gromos polarisable model for acetone. Mol Phys. 2016;114:845–854.

[26] Lavino A, Banetta L, Carbone P, et al. Extended charge-on-particle optimized potentials for liquid simulation acetone model: the case of acetone-water mixtures. J Phys Chem B. 2018;122:5234–5241.

[27] Faginas Lago N, Albertí M, Lombardi A, et al. A force field for acetone: the transition from small clusters to liquid phase investigated by molecular dynamics simulations. Theor Chem Acc. 2016;135:161.

[28] Perera A, Sokolić F. Modeling nonionic aqueous solutions: the acetone-water mixture. J Chem Phys. 2004;121:11272.

[29] Jorgensen W, Madura J, Swenson C. Optimized intermolecular potential functions for liquid hydrocarbons. J Am Chem Soc. 1984;106:6638.

[30] Duffy E, Severance D, Jorgensen W. Solvent effects on the barrier to isomerization for a tertiary amide from ab initio and monte carlo calculations. J Am Chem Soc. 1992;114:7535.

[31] Hansen JP, McDonald I. Theory of simple liquids. 3rd ed. Amsterdam: Academic Press, Elsevier; 2006.

[32] Lebowitz J, Percus J. Long-range correlations in a closed system with applications to nonuniform fluids. Phys Rev. 1961;122:1675.

[33] Kežić B, Perera A. Revisiting aqueous-acetone mixtures through the concept of molecular emulsions. J Chem Phys. 2012;137:134502.

[34] Kirkwood J, Buff F. The statistical mechanical theory of solutions. I. J Chem Phys. 1951;19:774.

[35] Ben-Naim A. Molecular theory of solutions. New York (NY): Oxford University Press; 2006.

[36] Ben-Naim A. Inversion of the Kirkwood-Buff theory of solutions: application to the water-ethanol system. J Chem Phys. 1977;67:4884.

[37] Matteoli E, Lepori L. Solute-solute interactions in water. II. An analysis through the Kirkwood-Buff integrals for 14 organic solutes. J Chem Phys. 1984;80:2856.

[38] Oran Brigham E. The fast Fourier transform. Upper Saddle River (NJ): Prentice-Hall, Inc; 1988.

[39] Wallace D. On the role of density fluctuations in the entropy of a fluid. J Chem Phys. 1987;87:2282–2284.

[40] Mountain R, Raveché H. Entropy and molecular correlation functions in open systems. II. Two- and three-body correlations. J Chem Phys. 1971;55(5):2250–2255.

[41] Baranyai A, Evans D. Direct entropy calculation from computer simulation of liquids. Phys Rev A. 1989;40:3817–3822.

[42] Laird B, Wang J, Haymet A. Consistent integral equations for two- and three-body-force models: application to a model of silicon. Phys Rev E. 1993;47:2491–2502.

[43] Lazaridis T, Karplus M. Orientational correlations and entropy in liquid water. J Chem Phys. 1996;105 (10):4294–4316.

[44] Wang L, Abel R, Friesner R, et al. Thermodynamic properties of liquid water: an application of a nonparametric approach to computing the entropy of a neat fluid. J Chem Theory Comput. 2009;5(6):1462–1473. PMID: 19851475.

[45] Lazaridis T. Inhomogeneous fluid approach to solvation thermodynamics. 1. Theory. . J Phys Chem B. 1998;102(18):3531–3541.

[46] Henao A, Johnston A, Guardia E, et al. On the positional and orientational order of water and methanol around indole: a study on the microscopic origin of solubility. Phys Chem Chem Phys. 2016;18:23006–23016.

[47] Silverstein K, Dill K, Haymet A. Hydrophobicity in a simple model of water: entropy penalty as a sum of competing terms via full, angular expansion. J Chem Phys. 2001;114(14):6303–6314.

[48] Fu CF, Tian SX. Different aggregation dynamics of benzene-water mixtures. Phys Chem Chem Phys. 2014;16:21957–21963.

[49] van der Spoel D, Lindahl E, Hess B, et al. Gromacs: fast, flexible, and free. J Comput Chem. 2005;26:1701.

[50] Martínez J, Martínez L. Packing optimization for automated generation of complex system's initial configurations for molecular dynamics and docking. J Comput Chem. 2003;24:819.

[51] Parrinello M, Rahman A. Crystal structure and pair potentials: a molecular-dynamics study. Phys Rev Lett. 1980;45:1196.

[52] Parrinello M, Rahman A. Polymorphic transitions in single crystals: a new molecular dynamics method. J Appl Phys. 1981;52:7182.

[53] Bussi G, Donadio D, Parrinello M. Canonical sampling through velocity rescaling. J Chem Phys. 2007;126:014101.

[54] Darden T, York D, Pedersen L. Particle mesh Ewald: an n*log(n) method for Ewald sums in large systems. J Chem Phys. 1993;98:10089.

[55] Jorgensen W, Maxwell D, Tirado-Rives J. Development and testing of the opls all-atom force field on conformational energetics and properties of organic liquids. J Am Chem Soc. 1996;118:11225.

[56] Wick C, Martin M, Siepmann J. Transferable potentials for phase equilibria. 4. United-atom description of linear and branched alkenes and alkylbenzenes. J Phys Chem B. 2000;104:8008.

[57] Jorgensen W. Optimized intermolecular potential functions for liquid alcohols. J Phys Chem. 1986;90:1276–1284.

[58] Lide DR editor. Crc handbook of chemistry and physics. 90th ed. (cd-rom version 2010). Boca Raton, FL: CRC Press/Taylor and Francis; 2010.

[59] Bushuev YG, Davletbaeva SV. Structural properties of liquid acetone. Russ Chem Bull. 1999;48:25.

[60] Cordeiro J. Structure of acetone and dimethyl sulfoxide from Monte Carlo simulations and MM2 calculations. Phys Chem Liq. 2007;45:31.

[61] Bertagnolli H, Hoffmann M, Ostheimer M. The intermolecular structure of acetone in the liquid state deduced from X-ray and neutron diffraction measurements and structure modelling technique. Z Phys Chem. 1989;165:165.

[62] Jónsson H, Andersen H. Icosahedral ordering in the Lennard-Jones liquid and glass. Phys Rev Lett. 1988;60:2295.

[63] Pugnaloni L, Vericat F. New criteria for cluster identification in continuum systems. J Chem Phys. 2002;116:1097.

[64] Benmore C, Loh Y. The structure of liquid ethanol: a neutron diffraction and molecular dynamics study. J Chem Phys. 2000;112:5877–5883.

[65] Murdoch K, Ferris T, Wright J, et al. Infrared spectroscopy of ethanol clusters in ethanol-hexane binary solutions. J Chem Phys. 2002;116:5717–5724.

[66] Kirkwood J, Lewinson V, Alder B. Radial distribution functions and the equation of state of fluids composed of molecules interacting according to the Lennard–Jones potential. J Chem Phys. 1952;20:929.

[67] Zoranić L, Sokolić F, Perera A. Microstructure of neat alcohols: a molecular dynamics study. J Chem Phys. 2007;127:024502.

[68] Perera A, Sokolić F, Zorani L. Microstructure of neat alcohols. Phys Rev E. 2007;75:060502.

[69] Ploetz E, Bentenitis N, Smith P. Kirkwood-Buff integrals for ideal solutions. J Chem Phys. 2010;132:164501.

[70] Ploetz E, Smith P. A Kirkwood-Buff force field for the aromatic amino acids. Phys Chem Chem Phys. 2011;13:18154–18167.

[71] Zoranić L, Sokolić F, Perera A. Density and energy distribution in water and organic solvents: a molecular dynamics study. J Mol Liq. 2007;136:199–205.

[72] Perera A, Zoranić L, Sokolić F, et al. A comparative molecular dynamics study of water-methanol and acetone-methanol mixtures. J Mol Liq. 2011;159:52–59.

[73] Polok K, Gadomski W, Sokolić F, et al. Molecular dynamics simulations and femtosecond optical kerr effect spectroscopy of methanol/acetone mixtures. J Mol Liq. 2011;159:60–69.

[74] Schäfer K, Rohr F. Kalorische untersuchungen an mischungen von aceton mit normal-kohlenwasserstoffen. Z Phys Chem. 1960;24:130–151.

[75] Campbell A, Kartzmark E. Thermodynamic and other properties of methanol + acetone, carbon disulphide + acetone, carbon disulphide + methanol, and carbon disulphide + methanol + acetone. J Chem Thermodyn. 1973;5:163–172.

[76] Saini R, Keum YS. Carotenoid extraction methods: a review of recent developments. Food Chem. 2018;240:90–103.